

**Interaction of bubbles in an inviscid and low-viscosity shear flow**Jai Prakash,<sup>\*</sup> Olga M. Lavrenteva,<sup>†</sup> and Avinoam Nir<sup>‡</sup>*Department of Chemical Engineering, Technion-Israel Institute of Technology, Haifa 32000, Israel*

(Received 2 June 2013; revised manuscript received 30 July 2013; published 21 August 2013)

The pressure loads on two identical spherical bubbles impulsively introduced in an inviscid simple shear flow are calculated. The interaction force due to these pressure loads is employed to model the dynamics of air bubbles injected to a low-viscosity fluid sheared in a Couette device at the first shear flow instability where the bubbles are trapped inside the stable Taylor vortex. It was shown that the interaction between the bubbles in the primary shear flow drives them away from each other. The performed simulations revealed that in an inviscid flow the separation distances between equal size bubbles undergo complex periodic motion. The presence of low-viscosity results in a qualitative change of the interaction pattern: The bubbles either eventually assume an ordered string with equal separation distances between all neighbors or some of them collide. The first regime is qualitatively similar to the behavior of bubbles at low Reynolds number [Prakash *et al.*, *Phys. Rev. E* **87**, 043002 (2013)]. Furthermore, if the Reynolds number exceeds some critical value the temporal behavior of the separations becomes nonmonotonic and exhibits over- and undershooting of the equilibrium separations. The latter effects were observed in the experiments, but are not predicted by the low Reynolds number model of the process [Prakash *et al.*, *Phys. Rev. E* **87**, 043002 (2013)].

DOI: 10.1103/PhysRevE.88.023021

PACS number(s): 47.15.ki, 47.55.dd

**I. INTRODUCTION**

Bubbles embedded in intensive vortical flow often exhibit complicated behavior; e.g., they may be trapped by vortices and form ordered structures. The study of such phenomena is of fundamental significance in several branches of fluid mechanics such as two-phase or bubbly flows. Examples of application of such flows can be found in, e.g., Magnaudet and Eames [1] and Climent *et al.* [2]. The flow in a Couette-Taylor device serves as a laboratory model of complex vortical flows. Deng *et al.* [3] reported an experimental study of the behavior of individual bubbles embedded in a Couette-Taylor flow at Reynolds numbers, corresponding to the first classical instability. It was observed that the bubbles are trapped either near the wall at stagnation points or in the vortex core and that equal size bubbles trapped in the core eventually assume an ordered string with equal separation distances between all neighbors. Experiments performed in our laboratory (Byk *et al.* [4], Prakash *et al.* [5]) reproduced these results, provided detailed measurements of the process evolution, and suggested a range of simplified models for the bubbles dynamics. Byk *et al.* [4] computed the force acting on two circles in a simple shear flow of an inviscid liquid in two-dimensional (2D) geometry and demonstrated that the interaction force is repulsive and decays relatively fast with the separation distance  $d$  as  $1/d^5$ . Prakash *et al.* [5] used the reciprocal theorem to calculate the leading order inertia-induced forces on two identical spherical bubbles in a simple shear flow at small but finite Reynolds numbers where viscous effects are dominant. This force was further employed to model bubbles interaction in a Couette-Taylor device and the results of simulations were compared with the experimental measurements. The Reynolds numbers (at the bubble scale) in the experiments were of

$O(1)$ , while the developed theory assumes small values of  $Re$ . Nevertheless, the results of computations proved to be in good agreement with the experimental observations; i.e., they describe the main effect of approaching the equilibrium position and provide a good measure of the evolution relaxation time. Nevertheless, some interesting phenomena that were observed in several experimental runs at various rotation velocities with two bubbles, such as the overshooting of the equilibrium separation or the reversal of the relative bubble motion and their eventual collision (see [5]), were not reproduced.

In this paper, we study the interaction of identical spherical bubbles in a simple shear flow when inertia is dominant, which is opposite to the case considered in [5]. The conditions at noncontaminated bubble boundaries can be approximated as free slip that allows approximating real fluids as inviscid in high Reynolds number bubble flows (Magnaudet and Eames [1], Legendre and Magnaudet [6]) and aeroacoustics (Howe [7]). A brief review of the results on the motion and interaction of solid and fluid particles in inviscid flow is given below.

The special cases of spheres in potential flows and of circles in 2D vortical ambient flows can be found in the classical literature (Lamb [8], Batchelor [9]). The generalization of these results to arbitrary body shapes and arbitrary potential flow fields are given in Landweber and Miloh [10] and Galper and Miloh [11,12].

Most of the studies of bodies translating in a rotational flow are devoted to the determination of a transverse or a lift force exerted on it. Auton [13] and Auton *et al.* [14] calculated the secondary velocity field induced by the vorticity and evaluated the resulting lift force on a sphere translating in a fully developed stationary rotational disturbance field. Their results were further extended to an arbitrarily shaped body (Catlin [15]). Another series of works concerns the force and torque on 3D bodies impulsively introduced in rotational flow. Legendre and Magnaudet [6] found the force on a sphere in an impulsively started linear shear flow. Miloh [16] determined the force and torque on an arbitrarily shaped deforming body

<sup>\*</sup>ceranjp@technix.technion.ac.il<sup>†</sup>ceolga@technix.technion.ac.il<sup>‡</sup>avinir@technix.technion.ac.il

in an ambient flow with uniform vorticity. Catlin [17] derived dynamical equations for freely deforming bodies with more than six degrees of freedom which are immersed in an inviscid incompressible flow with uniform vorticity but otherwise arbitrary nonuniform strain rate at the instant after the body was impulsively introduced into the fluid.

In this paper, we obtain the forces exerted on multiple spherical bubbles moving along a streamline in a simple inviscid shear flow and employed these to develop a simplified model of interaction of bubbles in a Couette-Taylor device. Note that a multibody system can be regarded as a single deformable body and, thus, the methods of [16,17] can be directly applied to such configurations. However, in view of the high symmetry of the system under consideration, we prefer to use a classical approach with explicit determination of the pressure and integrate it over the surface of each particle.

The paper is organized as follows. In Sec. II, the problem of the interaction of two spherical bubbles in a simple inviscid shear flow is formulated. Two methods are applied to construct the solutions and the results for the forces acting on the bubbles are presented. In Sec. III, two simplified models, inviscid and low-viscosity models, of the dynamics of bubbles in a Couette-Taylor device are formulated and discussed. Sections III A and III B present the results for bubble dynamics according to the inviscid and low-viscosity models, respectively, for a range of governing parameters. Separate attention is given to the behavior of the solutions of the inviscid and low-viscosity models in the vicinity of equilibrium and to the dynamic simulations according to the complete nonlinear equations, respectively. In Sec. IV, we summarize the results of the calculations and discuss their applicability to the experiments in the Couette-Taylor device.

## II. TWO BUBBLES IN A SIMPLE SHEAR FLOW

### A. Formulation of the problem

Consider two spherical bubbles of equal radii  $a$  impulsively introduced into an unbounded incompressible inviscid fluid of uniform density  $\rho$ , which is subjected to a simple shear flow  $\mathbf{v}^* = (0, 0, Gx^*)$  along the  $z$  axis, where  $G$  is the shear rate. The bubbles are assumed to be positioned on the same streamline  $x = y = 0$  at some initial separation and have some initial velocities in the  $z$  direction that are not necessarily equal.

In the following analysis time, length, velocity, and pressure will be nondimensionalized using  $1/G, a, Ga$ , and  $\rho G^2 a^2$ , respectively. Let  $\Omega$  be the domain occupied by the continuous fluid with  $\Gamma_i, i = 1, 2$  denoting the boundary of bubble  $i$ , and  $d$  be the distance between the centers of the bubbles (see Fig. 1). Let  $\mathbf{v}, \boldsymbol{\omega} = \nabla \times \mathbf{v}$ , and  $p$  denote the scaled velocity, vorticity, and pressure fields around the bubbles that are governed by the Euler equations:

$$\frac{\partial \mathbf{v}}{\partial t} + \nabla \left( \frac{\mathbf{v} \cdot \mathbf{v}}{2} \right) + \boldsymbol{\omega} \times \mathbf{v} = -\nabla p, \quad (1)$$

$$\nabla \cdot \mathbf{v} = 0, \quad \mathbf{x} \in \Omega. \quad (2)$$

Let bubble  $i, i = 1, 2$  translate with velocity  $\mathbf{v}_i = (0, 0, v_i)$  in a laboratory reference frame. In this reference frame, the velocity at the boundaries of the bubbles,  $\Gamma_1$  and  $\Gamma_2$ , and far

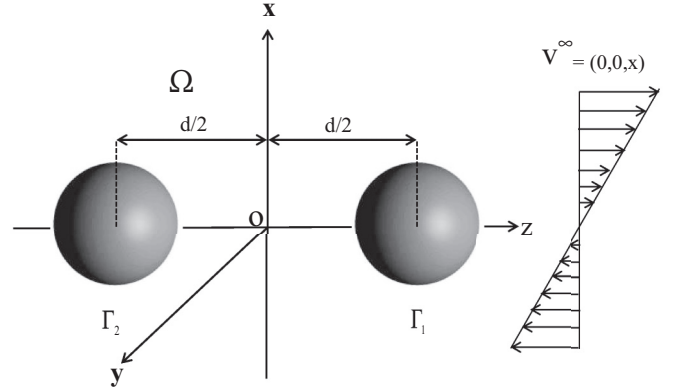


FIG. 1. Geometry of the problem.

from the inclusions satisfy

$$\mathbf{v} \cdot \mathbf{n} = \mathbf{v}_i \cdot \mathbf{n}, \quad \mathbf{x} \in \Gamma_i, i = 1, 2, \quad (3)$$

$$\mathbf{v} \rightarrow \mathbf{v}^\infty \quad \text{as} \quad |\mathbf{x}| \rightarrow \infty, \quad (4)$$

respectively, where  $\mathbf{v}^\infty = (0, 0, x)$ .

The problem is completed by specifying initial conditions for the velocity field that should satisfy (3) and (4). A popular choice of initial conditions assumes that the introduction of the bubbles does not alter the vorticity field that remains uniform and that the velocity field can be decomposed into irrotational and rotational components ([16]),

$$\mathbf{v} = \nabla \Phi + \mathbf{v}^\infty, \quad (5)$$

where the potential  $\Phi$  satisfies

$$\nabla^2 \Phi = 0, \quad (6)$$

$$\nabla \Phi \cdot \mathbf{n} + \mathbf{v}^\infty \cdot \mathbf{n} = \mathbf{v}_i \cdot \mathbf{n}, \quad \mathbf{x} \in \Gamma_i, i = 1, 2, \quad (7)$$

$$\Phi \rightarrow 0 \quad \text{as} \quad |\mathbf{x}| \rightarrow \infty. \quad (8)$$

Since the problem for the potential is linear it, in turn, can be decomposed into parts corresponding to shear flow and translation of the bubbles,

$$\Phi = \Phi^{\text{shear}} + \Phi^{\text{trans}} = \Phi^{\text{shear}} + \sum_{i=1}^2 v_i \Phi_i^{\text{trans}}, \quad (9)$$

where  $\Phi^{\text{shear}}, \Phi^{\text{trans}}$  are harmonic functions that decay at infinity and satisfy the following boundary conditions:

$$\nabla \Phi^{\text{shear}} \cdot \mathbf{n} + \mathbf{v}^\infty \cdot \mathbf{n} = 0, \quad \mathbf{x} \in \Gamma_i, i = 1, 2, \quad (10)$$

$$\nabla \Phi^{\text{trans}} \cdot \mathbf{n} = \mathbf{v}_i \cdot \mathbf{n}, \quad \mathbf{x} \in \Gamma_i. \quad (11)$$

The determination of the velocity field is thus reduced to a number of Neumann problems for the Laplace equation. The methods to solve these are well developed and we briefly describe the ones employed in this study in Sec. II B.

The net force exerted on bubble  $i$  by the flow can be obtained by integrating  $p\mathbf{n}$  over its surface, i.e.,

$$\mathbf{F}_i = - \oint_{\Gamma_i} p \mathbf{n} dS. \quad (12)$$

This force can be decomposed as

$$\mathbf{F}_i = \mathbf{F}_i^m + \mathbf{F}_i^{\text{lift}} + \mathbf{F}_i^{\text{int}} + \mathbf{F}_i^{\text{shear}}, \quad (13)$$

where  $\mathbf{F}_i^m$  is the added mass force, which depends linearly on the accelerations of the bubbles,  $\mathbf{F}_i^{\text{lift}}$  is the transversal lift force proportional to the vector product of the vorticity and velocity of the bubble relative to the fluid,  $\mathbf{F}_i^{\text{int}}$  arises due to the interaction of inclusions and is a quadratic function of the translation velocities, and  $\mathbf{F}_i^{\text{shear}}$  is due to the interaction of bubbles with the ambient flow that does not depend on their velocities.

Equating the force exerted on each bubble to zero (note that the density of the bubbles is negligible compared to that of the ambient fluid) provides two relations between the accelerations of the bubbles, their velocities and their relative positions, which are linear with respect to accelerations.

The added mass force  $\mathbf{F}_i^m$  and the interaction forces  $\mathbf{F}_i^{\text{int}}$  are determined solely by the irrotational component of the velocity field and the expressions for it can be found elsewhere, e.g., in Galper and Miloh [18]. The lift force  $\mathbf{F}_i^{\text{lift}}$  was the subject of numerous studies. The results for a single sphere (that is, the leading order contribution in the case of widely separated particles) are obtained in Auton *et al.* [14] and the more general case was considered by Miloh [16]. The last term  $\mathbf{F}_i^{\text{shear}}$  is quadratic in the vorticity of the ambient flow and was ignored in early studies based on *a priori* assumption of weak vorticity. Miloh [16,19] obtained this force for an arbitrary deformable body. Catlin [17] derived expressions for the force moments of any order. Since multibody system can be regarded as a single deformable body (see Galper and Miloh [18]) these results, in principle, can be employed to obtain the forces exerted on individual particles in the system. However, we prefer to derive these individual forces directly from the equations of motion and boundary conditions.

Further in this section, we concentrate on the determination of  $\mathbf{F}_i^{\text{shear}}$ . It is readily seen that this is the force exerted on a stationary bubble submerged in a simple shear flow in the presence of another stationary bubble, i.e., when  $\mathbf{v}_1 = \mathbf{v}_2 = \mathbf{0}$ . We assume that the velocity field of the form (5) is known and derive the expression for the pressure field. The latter requires the knowledge of the instantaneous velocity field as well as of the solenoidal instantaneous acceleration field  $\mathbf{v}_t$ . We look for this field in the form

$$\mathbf{v}_t = -(\boldsymbol{\omega} \times \mathbf{v}) + \nabla(H + Q), \quad (14)$$

where the auxiliary function  $Q$  satisfies Poisson equation

$$\nabla^2 Q = \nabla \cdot (\boldsymbol{\omega} \times \mathbf{v}) = \nabla \cdot (\boldsymbol{\omega} \times \mathbf{v}^\infty) = -1, \quad \mathbf{x} \in \mathbb{R}^3, \quad (15)$$

while  $H$  is harmonic in  $\Omega$  and satisfies the boundary condition

$$\nabla H \cdot \mathbf{n} = (\boldsymbol{\omega} \times \mathbf{v}) \cdot \mathbf{n} - \nabla Q \cdot \mathbf{n}, \quad \mathbf{x} \in \Gamma_i, i = 1, 2. \quad (16)$$

After substituting (14) into the Euler equation (1) the latter can be integrated and provide an explicit expression for the pressure field

$$p = p_0 - \left(\frac{1}{2}|\mathbf{v}|^2 + H + Q\right), \quad (17)$$

where  $p_0$  is a constant and  $Q = -\frac{x^2}{2}$ .

Note that these considerations are based on the assumption of a uniform vorticity that is valid only initially, or during a short time interval, before vortex stretching effects become

important. However, as argued in Miloh [16], the case of a body moving in an infinite expanse of fluid undergoing a simple shearing motion at infinity can be considered as an effectively inviscid flow with uniform vorticity.

## B. Method of solution

We present the solution of two bubbles of equal radii embedded in a simple shear flow of an inviscid liquid. We adopt two methods, namely, approach via bispherical coordinates, which yields an exact solution of the problem, corroborated by the method of reflections, which provides an approximate solution of the given problem. Following Lebedev [20] the general solution for potential, which satisfies Laplace equation, is presented in the form of a series in bispherical harmonics, and the coefficients of the series are determined from the boundary conditions. The details of this procedure are presented in the Appendix. Below, we briefly present the Schwarz alternating method, or the so called method of reflections (see, e.g., Courant and Hilbert [21] or Happel and Brenner [22] for more details).

We present the solution for the potentials  $\Phi^{\text{shear}}$ ,  $\Phi^{\text{trans}}$  and  $H$  in the case where velocities and accelerations of the bubbles are directed along the  $z$  axis using the approximate method of reflections. For the two spherical bubbles in Fig. 2, the solution is presented in the form

$$\begin{aligned} \Phi^{\text{shear}} &= \sum_{i=1}^2 \sum_{k=1}^{\infty} \Phi_{i,k}^{\text{shear}}(r_i, \theta_i, \phi), \\ \Phi^{\text{trans}} &= \sum_{i=1}^2 \sum_{k=1}^{\infty} \Phi_{i,k}^{\text{trans}}(r_i, \theta_i, \phi), \\ H &= \sum_{i=1}^2 \sum_{k=1}^{\infty} H_{i,k}(r_i, \theta_i, \phi), \end{aligned} \quad (18)$$

where  $(r_i, \theta_i, \phi)$  are spherical coordinate systems originating at the center of bubble  $i$  (Fig. 2) and  $k$  indicates the number of reflections. Here,  $\Phi_{i,k}^{\text{shear}}$ ,  $\Phi_{i,k}^{\text{trans}}$ , and  $H_{i,k}$  are harmonic in the domain  $r_i > 1$ , decaying at infinity, with  $\Phi_{i,0}^{\text{shear}}$ ,  $\Phi_{i,0}^{\text{trans}}$ , and  $H_{i,0}$  satisfying the conditions (10), (11), and (16) at  $r_i = 1$ ,

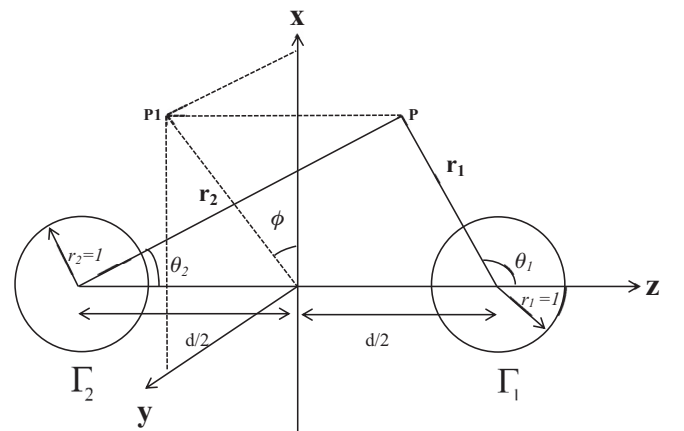


FIG. 2. Spherical coordinate systems connected to two bubbles. P1 is the projection of point P on the  $x$ - $y$  plane.

respectively, while

$$\nabla \Phi_{i,k+1}^{\text{shear}} \cdot \mathbf{n} = -\nabla \Phi_{j,k}^{\text{shear}} \cdot \mathbf{n}, \quad \mathbf{x} \in \Gamma_i, \quad i \neq j, \quad (19)$$

$$\nabla \Phi_{i,k+1}^{\text{trans}} \cdot \mathbf{n} = -\nabla \Phi_{j,k}^{\text{trans}} \cdot \mathbf{n}, \quad \mathbf{x} \in \Gamma_i, \quad i \neq j, \quad (20)$$

$$\nabla H_{i,k+1} \cdot \mathbf{n} = -\nabla H_{j,k} \cdot \mathbf{n}, \quad \mathbf{x} \in \Gamma_i, \quad i \neq j. \quad (21)$$

It is easy to show that

$$\begin{aligned} \Phi^{\text{shear}} = & \frac{1}{6d^4} \left( \frac{\sin \theta_1}{r_1^2} - \frac{\sin \theta_2}{r_2^2} \right) \cos \phi + \frac{1}{3} \left( 1 - \frac{8}{3d^5} \right) \left( \frac{\sin \theta_1 \cos \theta_1}{r_1^3} + \frac{\sin \theta_2 \cos \theta_2}{r_2^3} \right) \cos \phi \\ & + \frac{15}{24d^6} \left[ \frac{(5 \cos^2 \theta_1 - 1) \sin \theta_1}{r_1^4} - \frac{(5 \cos^2 \theta_2 - 1) \sin \theta_2}{r_2^4} \right] + O\left(\frac{1}{d^7}\right), \end{aligned} \quad (22)$$

and

$$\begin{aligned} \Phi^{\text{trans}} = & -\frac{1}{2} \left( \frac{v_1 \cos \theta_1}{r_1^2} + \frac{v_2 \cos \theta_2}{r_2^2} \right) + \frac{1}{2d^3} \left( \frac{v_2 \cos \theta_1}{r_1^2} + \frac{v_1 \cos \theta_2}{r_2^2} \right) - \frac{1}{2d^4} \left[ \frac{v_2(3 \cos^2 \theta_1 - 1)}{r_1^3} - \frac{v_1(3 \cos^2 \theta_2 - 1)}{r_2^3} \right] \\ & + \frac{3}{4d^5} \left[ \frac{v_2(5 \cos^3 \theta_1 - 3 \cos \theta_1)}{r_1^4} + \frac{v_1(5 \cos^3 \theta_2 - 3 \cos \theta_2)}{r_2^4} \right] + O\left(\frac{1}{d^6}\right), \end{aligned} \quad (23)$$

and the auxiliary potential  $H$ ,

$$\begin{aligned} H = & -\frac{1}{12d^4} \left( \frac{\cos \theta_1}{r_1^2} - \frac{\cos \theta_2}{r_2^2} \right) - \frac{1}{18} \left( 1 - \frac{8}{3d^5} \right) \left[ \frac{(3 \cos^2 \theta_1 - 1)}{r_1^3} + \frac{(3 \cos^2 \theta_2 - 1)}{r_2^3} \right] \\ & + \frac{1}{18} \left( 1 - \frac{6}{d^5} \right) \left( \frac{\sin^2 \theta_1}{r_1^3} + \frac{\sin^2 \theta_2}{r_2^3} \right) \cos 2\phi - \frac{5}{16d^6} \left[ \frac{(5 \cos^3 \theta_1 - 3 \cos \theta_1)}{r_1^4} - \frac{(5 \cos^3 \theta_2 - 3 \cos \theta_2)}{r_2^4} \right] \\ & + \frac{155}{96d^6} \left( \frac{\sin^2 \theta_1 \cos \theta_1}{r_1^4} - \frac{\sin^2 \theta_2 \cos \theta_2}{r_2^4} \right) \cos 2\phi + O\left(\frac{1}{d^7}\right). \end{aligned} \quad (24)$$

The various forces exerted on bubble 1, i.e., added mass force  $\mathbf{F}^m$ , force due to interaction  $\mathbf{F}^{\text{int}}$  and force due to shear flow  $\mathbf{F}^{\text{shear}}$  are obtained as

$$\mathbf{F}^m = -\frac{2\pi}{3} \left( \dot{v}_1 - \frac{3}{d^3} \dot{v}_2 \right) + O\left(\frac{1}{d^6}\right), \quad \mathbf{F}^{\text{int}} = \frac{6\pi v_2^2}{d^4} + O\left(\frac{1}{d^6}\right), \quad \mathbf{F}^{\text{shear}} = \frac{\pi}{3d^4} \left( 1 + \frac{80}{9d^2} \right) + O\left(\frac{1}{d^7}\right). \quad (25)$$

The shear force exerted on bubble 2 has the same magnitude but an opposite direction. The calculated shear force exerted on the bubbles is of a repulsive nature and it diminishes rapidly with the separation distance between the bubbles as  $1/d^4$ .

Variation of the force ( $\mathbf{F}^{\text{shear}}$ ) exerted on bubble 1 versus the separation distance is depicted in Fig. 3. The solid curve is calculated making use of bispherical coordinates. Dashed and dotted curves are calculated by the reflection method with the accuracy  $O(1/d^5)$  and  $O(1/d^6)$ , respectively. Note that at  $d > 3$ , with one radius of separation, both methods estimate the force in good agreement and the difference between the exact solution computed via bispherical coordinates and approximate one calculated by the reflection method, with the accuracy  $O(1/d^6)$ , does not exceed 5%, whereas with the accuracy  $O(1/d^5)$  and  $d > 10$  the difference does not exceed 10%.

Note that the generalization of the reflection method to the multibubble case is straightforward and that, at the leading order in  $1/d$ , the result is additive, i.e., the force on a bubble due to interaction with several others is the sum of forces resulting from pairwise interactions. Further in this paper

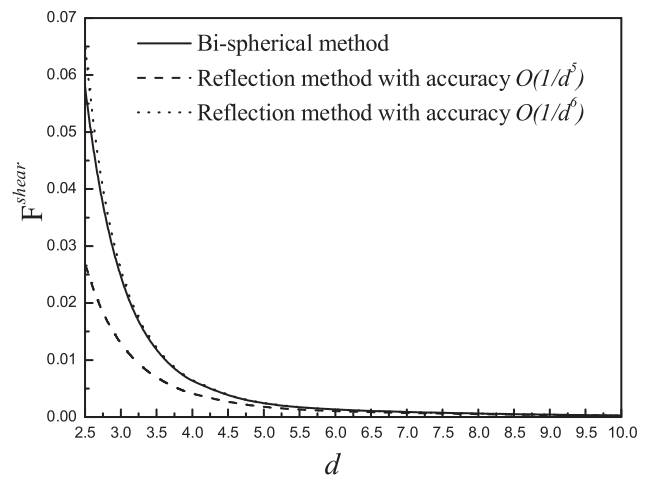


FIG. 3. Force exerted on the right bubble in a pair of bubbles embedded in a simple shear flow. The solid curve is calculated making use of bispherical coordinates. The dashed and dotted curves are calculated by the reflection method with the accuracy  $O(1/d^5)$  and  $O(1/d^6)$ , respectively.

we use approximate expressions for the forces obtained via reflections method.

### III. BUBBLE DYNAMICS IN A COUETTE-TAYLOR DEVICE

Consider  $N$  spherical bubbles of unit radii positioned along a center closed streamline in a stable Taylor vortex. Let  $l$  be the length of this streamline and  $l_n$  be the distance between the centers of the bubbles  $n$  and  $n + 1$ . It may be noted that the presence of  $N$  bubbles of unit radii implies that  $l > 2N$ . The distance between bubbles 1 and  $N$  can be written as

$$l_N = l - \sum_{n=1}^{N-1} l_n \quad (N \geq 2). \quad (26)$$

The values  $l_n$  change dynamically due to the repulsive shear force experienced by the bubbles embedded in the shear flow during their relative motion.

In order to apply the result obtained in Sec. II B to the dynamics of the bubbles in a Couette-Taylor device, we propose two simplified models of the process:

(A) an inviscid flow model where the force acting on the bubble arises purely from the variation of the pressure over the bubble surface;

(B) a low-viscosity model where viscous drag force exerted on the bubble tends to slow down its motion relative to the fluid.

The following assumptions are made in order to simplify these models.

(i) Bubble interaction is due to the primary shear flow. The Taylor vortex keeps the bubbles at the center streamline, preventing their rise either due to buoyancy or due to the transversal lift.

(ii) The primary flow is modeled by an unbounded unidirectional simple shear, neglecting nonzero curvature of the streamlines. This follows from the diminishingly small ratio of bubble to streamline radii in the experiments of [3–5].

(iii) In the definition of the model we defined the pressure as given in (17) neglecting deviation of vorticity from its initial uniform distribution in the undisturbed simple shear flow.

(iv) Each bubble interacts only with its nearest neighbors.

#### A. Inviscid flow model

##### 1. Governing equations

Following (13), the force balance on the bubbles has the form

$$\mathbf{F}_n^m + \mathbf{F}_n^{\text{int}} + \mathbf{F}_n^{\text{shear}} = \mathbf{0}, \quad n = 1, \dots, N, \quad (27)$$

where the forces are calculated taking into account the interaction of the  $n$ th bubble with its neighbors. Solving (25) and (27) with respect to accelerations, and keeping the leading terms, we obtain

$$\dot{v}_n = -9 \left\{ \frac{v_{n-1}^2}{l_{n-1}^4} - \frac{v_{n+1}^2}{l_n^4} \right\} + \frac{1}{2} \left\{ \frac{1}{l_n^4} - \frac{1}{l_{n-1}^4} \right\}, \quad (28)$$

where  $l_0 = l_N, v_0 = v_N$ , and  $v_{N+1} = v_1$ .

The temporal evolution of  $l_n$  is governed by

$$\frac{dl_n}{dt} = v_n - v_{n+1}, \quad n = 1, \dots, N. \quad (29)$$

Equations (28) and (29) comprise an ODE system of the order  $2N$  that should be solved with initial conditions for the velocities of the bubbles and the separations between them. It follows from (29) that  $\sum_{n=1}^N l_n$  is an integral of the system, thereby reducing the system to order  $2N - 1$ .

In the case of a two bubble system, the inviscid model (28) yields the following two equations, which result from the force balance on the two bubbles

$$\begin{aligned} \dot{v}_1 &= -9 \left\{ \frac{v_2^2}{(l-l_1)^4} - \frac{v_1^2}{l_1^4} \right\} + \frac{1}{2} \left\{ \frac{1}{l_1^4} - \frac{1}{(l-l_1)^4} \right\}, \\ \dot{v}_2 &= -9 \left\{ \frac{v_1^2}{l_1^4} - \frac{v_2^2}{(l-l_1)^4} \right\} + \frac{1}{2} \left\{ \frac{1}{(l-l_1)^4} - \frac{1}{l_1^4} \right\}. \end{aligned} \quad (30)$$

Introduction of new variables  $u = v_1 - v_2, v = v_1 + v_2$  simplifies Eqs. (29) and (30) to

$$\dot{v} = -9uv \left\{ \frac{1}{l_1^4} - \frac{1}{(l-l_1)^4} \right\}, \quad (31)$$

$$\dot{u} = \left[ 1 + \frac{9}{2}(u^2 + v^2) \right] \left\{ \frac{1}{l_1^4} - \frac{1}{(l-l_1)^4} \right\}, \quad (32)$$

$$\frac{dl_1}{dt} = u. \quad (33)$$

One can see that  $l_1 = l/2, u = 0, v = v_0 = \text{constant}$  is a stationary equilibrium solution of (31)–(33). Below we present the linear analysis separately to obtain an analytical solution in the vicinity of a stationary state followed by the numerical solution of the general nonlinear equations.

#### 2. Linearized solution near stationary state

Let

$$l_1 = \frac{l}{2} + \xi, \quad v = v_0 + \eta, \quad \xi, \eta, u \ll 1.$$

Linearization of (31)–(33) in the vicinity of a stationary solution results in

$$\dot{\xi} = u, \quad \dot{\eta} = 0, \quad \dot{u} = -2^8 l^{-5} \left( 1 + \frac{9}{2} v_0^2 \right) \xi. \quad (34)$$

The general solution of (34) is

$$\begin{aligned} \xi &= c_1 \sin \lambda t + c_2 \cos \lambda t, \quad \eta = c_3, \\ u &= c_1 \lambda \cos \lambda t - c_2 \lambda \sin \lambda t, \\ \lambda &= 2^4 \sqrt{l^{-5} \left( 1 + \frac{9}{2} v_0^2 \right)}. \end{aligned} \quad (35)$$

The solution is periodic; i.e., a stationary solution is a center, with the period increasing with the length of streamline and decreasing with the initial velocity of the bubbles relative to the fluid. It is evident that with the absence of any damping mechanism, i.e., for a bubble in an inviscid flow field, the separation distance, as well as the relative velocity, will sustain periodic oscillations indefinitely.

#### 3. Nonlinear effects

From Eq. (31), it can be concluded that if,  $v(0) = 0$ , then  $v = 0 \forall t > 0$ . In this case Eqs. (32) and (33) comprise a nonlinear second order autonomous system of differential

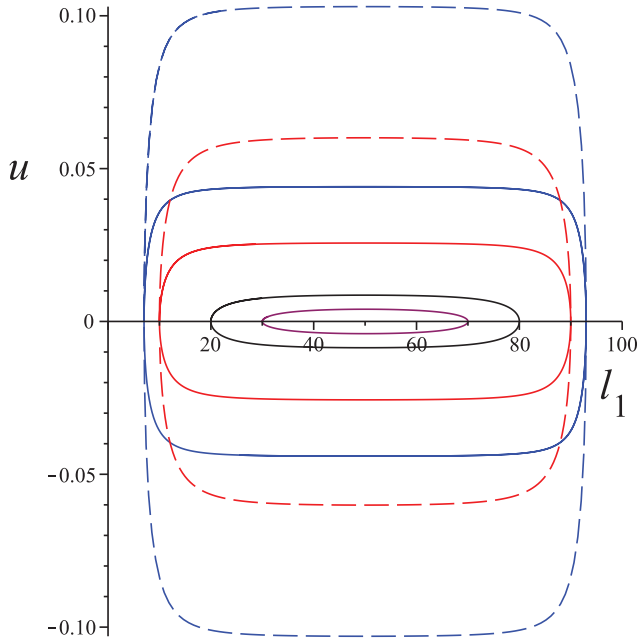


FIG. 4. (Color online) Effect of nonlinearity on the phase space pattern (two bubble case),  $l = 100$ . Solid lines correspond to the initial velocity  $v(0) = 0$ ; dashed lines correspond to the initial velocity  $v(0) = 1$ .

equations, which describes the evolution of the separation between two bubbles, that can be integrated analytically to yield

$$u = \pm \frac{1}{3} \sqrt{C_1 \exp \left[ -3 \frac{l(l^2 - 3ll_1 + 3l_1^2)}{l_1^3(l - l_1)^3} \right] - 2}, \quad (36)$$

where  $C_1$  is a constant of integration.

A phase portrait of this system with  $v(0) = 0$  and  $l = 100$  is shown in Fig. 4 by solid lines. Closed trajectories correspond to periodic solutions. It is evident that the phase lines (trajectories) in the vicinity of the stationary point resemble ellipses predicted by the linear theory. The nonlinearity of Eq. (32) manifests itself in the deformation of the phase lines far from equilibrium position. Dashed lines in Fig. 4 are projections of trajectories corresponding to (31)–(33) at  $v(0) = 1$ . One can see that the amplitude of oscillations for relative velocity is increased while for separation it remains almost the same.

For other cases, the system (31)–(33) was integrated numerically for various initial conditions. It was found that the separation distance shows a periodic behavior which continues uninterrupted, with the absence of a dissipative process, and no equilibrium is achieved. Sample evolution of separation is depicted in Fig. 5(a) at different initial separation distances  $l_1(0) = 20$  and  $l_1(0) = 30$ , where  $l = 100$ ,  $u(0) = 0$ ,  $v(0) = 0.15$ . Figure 5(b) shows the evolution of the composite velocity  $v(t)$ . One can see that the period of oscillation of  $v$  is considerably smaller than that of  $l_1$  and its derivative  $u$ . Also, in contrast to the solutions of the linearized equations, the period of oscillations depends strongly on the initial conditions, i.e., initial separations and velocities. This dependence on  $u$  and  $l_1$  is shown in Fig. 6. It can be seen that the period of the oscillations increases with the initial separation as

long as it does not exceed the equilibrium value but it decreases with initial velocities. When the initial relative velocity,  $u$ , is zero and the initial position approaches the equilibrium, the period tends to the value  $2^{-5/2} \pi \sqrt{l^5 / (2 + 9v_0^2)}$  predicted by the linear theory. For large initial deviation from the equilibrium position, the period is considerably shorter. Computations performed in cases of multiple (three and four) bubbles also demonstrated periodic motion.

## B. Low-viscosity model

### 1. Governing equations

In this section, we aim to discuss the effect of low viscosity on the evolution of the separation distances between the bubbles. The evolution of separation as discussed in the inviscid case undergoes periodic motion which continues indefinitely. We introduce a low viscous effect which produces a drag force that slows the motion of the bubbles, and eventually the bubbles assume equilibrium positions. In order to simplify the model we assume that the dynamics of the bubbles is governed by a balance between the added mass force, force due to primary shear flow, interaction force as in (27), and an additional viscous resistance due to the slow translation of the bubbles relative to the ambient fluid.

The first estimate of the viscous drag, translating with a velocity  $U$ , on a spherical bubble of radius  $a$  in the asymptotic limit of high Reynolds numbers was obtained by Levich [23, 24] from a balance between the rate of work done by the drag force and viscous dissipation within the fluid, and it has the dimensional form

$$\mathbf{F}^{\text{viscous}} = -12\pi\mu aU. \quad (37)$$

Kang and Leal [25] determined this drag force directly through the integration of the normal stress over the bubble surface and have shown that (37) is valid in the leading order in the Reynolds number. Stone [26] gave an alternative derivation of this result by showing that the steady drag experienced by a bubble or a drop of arbitrary shape moving in a uniform flow can be expressed in terms of volume and surface integrals of the vorticity field. For an inviscid spherical bubble, the result of Eq. (37) was recovered. Moore [27] obtained a correction to (37) in the steady case analyzing the flow in a thin boundary layer and in a narrow wake where the vorticity produced by the shear-free condition is confined, in the asymptotic limit of high Reynolds number. Chen [28] obtained the instantaneous viscous resistance force from the kinetic energy balance over the whole flow domain and determined the drag coefficient that tends to the result given by Moore for large time and found the leading order correction to (37) at small time. Slavchev and Simeonov [29] used a matched asymptotic expansion to find the short time velocity and pressure fields around the bubble. They evaluated the drag force through a direct integration of the stress on the bubble surface and obtained the next term in the expansion. They also considered a bubble accelerating uniformly from rest and showed that at short time, the drag force is essentially the sum of the added mass force and the viscous drag force given by (37), with the Reynolds number  $\text{Re}(t)$  based on the instantaneous slip velocity. Magnaudet and Legendre [30] examined the drag force on a bubble with a time-dependent radius,  $a(t)$ , and recovered (37) in the special

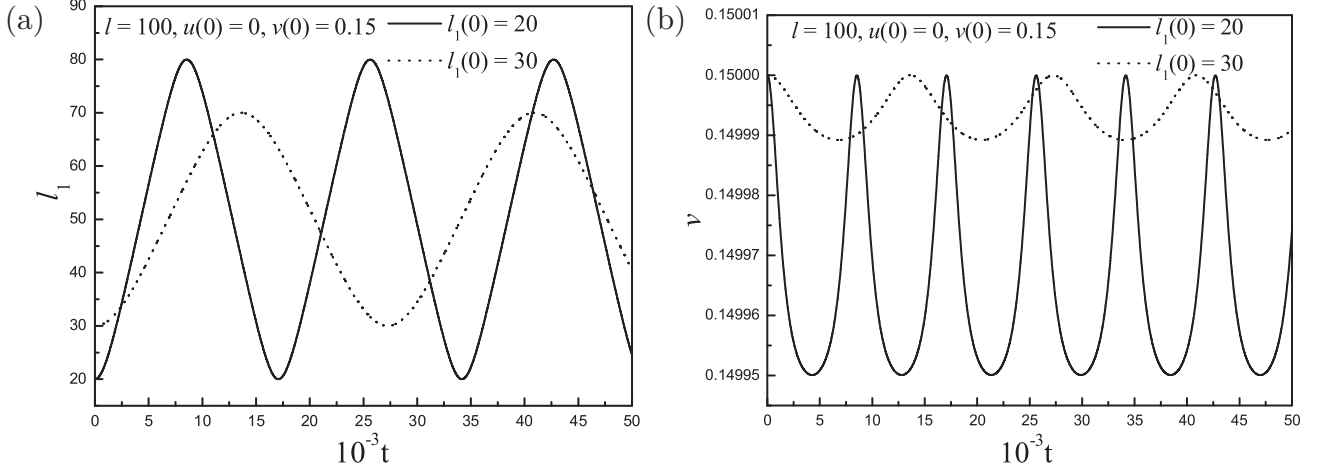


FIG. 5. Dynamics of evolution in the two bubble case: (a) separation distance between the bubbles, (b) composite velocity  $v$ .

case of a constant radius. More references on the subject can be found in Magnaudet and Eames [1].

The results reviewed above concern the drag on a single bubble in an unbounded fluid. To evaluate effect of multiple bubbles note that at large separations, the leading order perturbation of the flow in the vicinity of bubble 1 due to the motion of bubble 2 translating with velocity  $v_2$  is the same as that induced by a uniform flow at infinity with velocity  $3v_2/d^3$  [see Eq. (23)]. Thus, the scaled viscous resistance for bubble  $n$  in the presence of bubbles  $(n-1)$  and  $(n+1)$  takes the form [assuming that all the separations are large and are of the same order of magnitude  $l_n = O(d)$ ]

$$\mathbf{F}_n^{\text{visc}} = -\frac{12\pi}{\text{Re}} \left[ v_n - \frac{3v_{n+1}}{l_{n+1}^3} - \frac{3v_{n-1}}{l_n^3} + O\left(\frac{1}{d^4}\right) \right], \quad (38)$$

where  $\text{Re} = \rho Ga^2/\mu$  is the Reynolds number.

Similar to the inviscid case, we neglect the mass of the bubble and require that the net force exerted on it be zero. Thus, the force exerted on the  $n$ th bubble is balanced by added mass force, the force due to translation of neighbor bubbles and the viscous resistance given by (38). According to the assumptions of the model all the forces are calculated taking into account the presence of the  $(n-1)$ th and  $(n+1)$ th translating bubbles.

Force balances on all  $N$  bubbles provide  $N$  equations relating accelerations of the inclusions, their velocities, and separation distances. These equations are linear with respect to accelerations. Solving them with respect to bubble accelerations and neglecting the terms of the order  $\geq O(d^{-6})$ , we obtain the equations of motion in the form

$$\dot{v}_n = -9 \left\{ \frac{v_{n-1}^2}{l_{n-1}^4} - \frac{v_{n+1}^2}{l_n^4} \right\} + \frac{1}{2} \left\{ \frac{1}{l_n^4} - \frac{1}{l_{n-1}^4} \right\} - \frac{18}{\text{Re}} v_n, \quad (39)$$

$$\frac{dl_n}{dt} = v_n - v_{n+1}, \quad n = 1, \dots, N, \quad (40)$$

where  $l_0 = l_N, v_0 = v_N$ , and  $v_{N+1} = v_1$  and  $\text{Re}$  is the Reynolds number.

The equations of motion for the two bubble case, including the viscous effect, are given by

$$\dot{v} = -9uv \left[ \frac{1}{l_1^4} - \frac{1}{(l-l_1)^4} \right] - \frac{18}{\text{Re}} v, \quad (41)$$

$$\dot{u} = \left[ 1 + \frac{9}{2}(u^2 + v^2) \right] \left[ \frac{1}{l_1^4} - \frac{1}{(l-l_1)^4} \right] - \frac{18}{\text{Re}} u, \quad (42)$$

$$\frac{dl_1}{dt} = u, \quad (43)$$

where  $u = v_1 - v_2, v = v_1 + v_2$ .

It is easy to see that  $l_n = l/N, v_n = 0$  is a stationary equilibrium solution of (39) and (40) and  $l_1 = l/2, u = 0, v = 0$  is a stationary equilibrium solution of (41)–(43). Note that in contrast to the pure inviscid model, stationary solutions with arbitrary  $v$  are not possible. In the following section, we first study the behavior of solution in the vicinity of the equilibrium via solving corresponding linearized equations. The nonlinear effects are investigated via numerical solution of Eqs. (39)–(43).

## 2. Linearization near stationary solution

In the two bubble case linearization of (41)–(43) in the vicinity of stationary solution results in

$$\dot{\xi} = u, \quad \dot{u} = -\frac{18}{\text{Re}} u - 2^8 l^{-5} \xi, \quad \dot{v} = -\frac{18}{\text{Re}} v, \quad (44)$$

where  $l_1 = \frac{l}{2} + \xi, \xi, u, v \ll 1$ . The general solution of Eq. (44) is

$$\begin{aligned} \xi &= c_1 \exp(\lambda_1 t) + c_2 \exp(\lambda_2 t), \\ u &= c_1 \lambda_1 \exp(\lambda_1 t) + c_2 \lambda_2 \exp(\lambda_2 t), \\ v &= c_3 \exp\left(-\frac{18}{\text{Re}} t\right), \end{aligned} \quad (45)$$

where

$$\lambda_1 = -\frac{9}{\text{Re}} + \sqrt{\frac{81}{\text{Re}^2} - \frac{2^8}{l^5}}, \quad \lambda_2 = -\frac{9}{\text{Re}} - \sqrt{\frac{81}{\text{Re}^2} - \frac{2^8}{l^5}}.$$

One can see that, in the two bubble case, the magnitude of the composite translation velocity  $v$  decays exponentially, while for the separation distance and the relative velocity there exists a critical Reynolds number  $\text{Re}_{cr} = 9l^{5/2}/16$  below which these variables approach the equilibrium monotonically. If  $\text{Re} > \text{Re}_{cr}$ , both  $\lambda_1$  and  $\lambda_2$  are complex and the solution (45) exhibits an oscillatory behavior with exponentially decaying

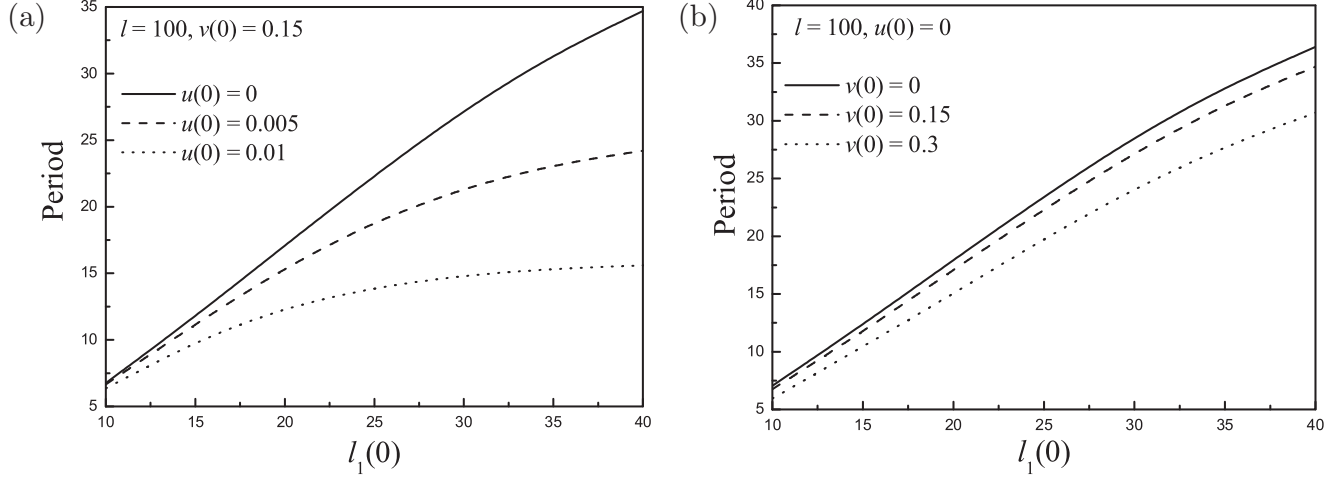


FIG. 6. Dependence of the period of oscillations on various initial conditions (two bubble case).

amplitude. We define the relaxation time  $T_{rel}$  in which the deviations from the equilibrium decrease tenfold. It follows from (45) that for supercritical Reynolds number,  $T_{rel} = Re/3$ . For subcritical Reynolds number  $Re < Re_{cr}$ , both  $\lambda_1$  and  $\lambda_2$  are real with  $\lambda_2 < \lambda_1 < 0$ , and the relaxation time in the subcritical system is defined by  $3/|\lambda_1|$ . In a subcritical situation the relaxation time grows monotonically with decreasing  $Re$ , and at  $Re \ll l^{5/2}$  it can be approximated by  $T_{rel} = 3/|\lambda_1| \simeq 27 \times 2^{-7} l^5 / Re$  [note that in experimental devices  $l \geq O(10^2)$ , see, e.g., [5], and thus the above inequality does not contradict the assumption of high  $Re$ ].

In the case of three bubbles, the stationary solution of (39) and (40) is  $l_1 = l_2 = l_3 = l/3, v_1 = v_2 = v_3 = 0$ . Linearization of (39) and (40) in the vicinity of the stationary solution, and introduction of new variables  $v = v_1 + v_2 + v_3, u_1 = v_1 - v_2, u_2 = v_2 - v_3$ , results in

$$\begin{aligned} \dot{\xi}_1 &= u_1, \quad \dot{\xi}_2 = u_2, \quad \dot{v} = -\frac{18}{Re}v, \\ \dot{u}_1 &= -\frac{18}{Re}u_1 - 2 \times 3^6 l^{-5} \xi_1, \\ \dot{u}_2 &= -\frac{18}{Re}u_2 - 2 \times 3^6 l^{-5} \xi_2, \end{aligned} \quad (46)$$

where  $l_1 = \frac{l}{3} + \xi_1, l_2 = \frac{l}{3} + \xi_2, \xi_1, \xi_2, u_1, u_2, v \ll 1$ . The general solution of Eq. (46) is

$$\begin{aligned} \xi_1 &= c_1 \exp(\lambda_3 t) + c_2 \exp(\lambda_4 t), \\ u_1 &= c_1 \lambda_3 \exp(\lambda_3 t) + c_2 \lambda_4 \exp(\lambda_4 t), \\ \xi_2 &= c_3 \exp(\lambda_3 t) + c_4 \exp(\lambda_4 t), \\ u_2 &= c_3 \lambda_3 \exp(\lambda_3 t) + c_4 \lambda_4 \exp(\lambda_4 t), \\ v &= c_5 \exp\left(-\frac{18}{Re}t\right), \end{aligned} \quad (47)$$

where

$$\begin{aligned} \lambda_3 &= -\frac{9}{Re} + \sqrt{\frac{81}{Re^2} - \frac{2 \times 3^6}{l^5}}, \\ \lambda_4 &= -\frac{9}{Re} - \sqrt{\frac{81}{Re^2} - \frac{2 \times 3^6}{l^5}}. \end{aligned}$$

One can see that, in this case also, the magnitude of the composite translation velocity  $v$  decays exponentially, while for the separation distances and the relative velocities there exists a critical Reynolds number  $Re_{cr} = l^{5/2}/3\sqrt{2}$ , below which these variables approach the equilibrium monotonically. Note that the critical Reynolds number in the three bubble case is considerably lower than in the two bubble case. If  $Re > Re_{cr}$ , both  $\lambda_3$  and  $\lambda_4$  are complex and the solution (47) exhibits an oscillatory behavior with exponentially decaying amplitude. It follows from (47) that, for supercritical  $Re$ ,  $T_{rel} = Re/3$ . For subcritical Reynolds number  $Re < Re_{cr}$ , both  $\lambda_3$  and  $\lambda_4$  are real. The relaxation time in the subcritical system is defined by  $3/|\lambda_3|$ . It monotonically grows with decreasing  $Re$ , and at  $Re \ll l^{5/2}$  and large  $l$ , it can be approximated by  $T_{rel} = 3/|\lambda_3| \simeq 3^{-3} l^5 / Re$ .

The relaxation time evaluated via the linearized equations is depicted in Fig. 7 versus  $Re$  for two (solid line with square markers) and three (solid line with circular markers) bubbles at  $l = 100$ . One can observe that, at subcritical Reynolds

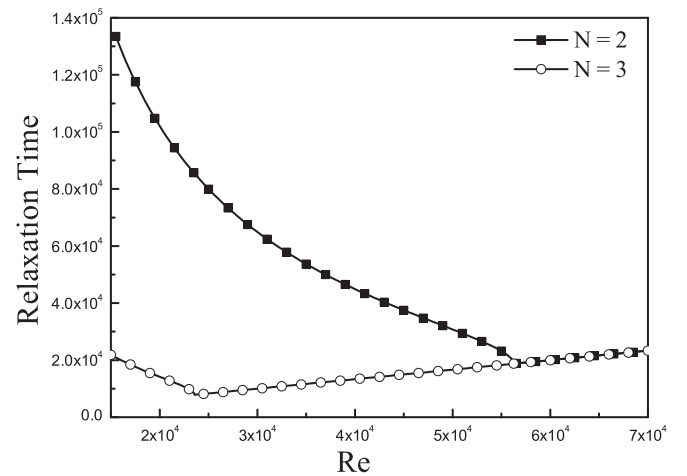


FIG. 7. Dependence of the relaxation time on the Reynolds number in the two and three bubble cases. The points at which the slope changes sign indicate the positions of critical Reynolds numbers.

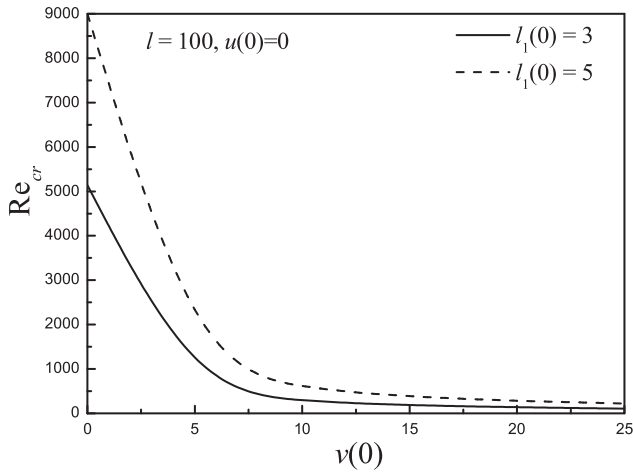


FIG. 8. Dependence of critical Reynolds number on various initial conditions (two bubble case).

numbers, the three bubble system exhibits a considerably faster relaxation than the two bubble system, while at supercritical situation, the relaxation time is almost independent of the number of bubbles. Also, the fastest relaxation takes place at critical Reynolds number.

Studying linearized systems with more than three bubbles revealed a complicated behavior with multiple modes of oscillations and damping. However, several qualitative features and trends remain similar: At nonzero viscosity, the solutions tend to equilibrium, there is a critical Reynolds number that grows with the parameter  $l$  and decreases with the number of bubbles, and the relaxation time decreases with the number of bubbles especially at subcritical situation.

### 3. Nonlinear effects

The nonlinear effects were studied via numerical integration of the system (39) and (40). It was demonstrated that, as anticipated and predicted by the linear analysis, the presence of the viscous force causes a damping effect, the oscillations die out in time, and the bubbles assume equilibrium positions. There exists a critical Reynolds number beyond which the evolution exhibits nonmonotonic behavior that grows fast with  $l$ . However, in contrast to the results based on the linearization, where the critical Reynolds number depends solely on the parameter  $l$  and on the number of bubbles in the system, the computations of the nonlinear system of equations reveal dependence on the initial conditions, i.e., separations and velocities. These effects are demonstrated in Fig. 8, where  $l = 100$ ,  $u(0) = 0$ , and  $l_1(0) = 3$  and 5. One can see that the critical Reynolds number increases with the initial separation  $l_1(0)$ .

Note that at small values of  $v(0)$ , the critical Reynolds number is much higher than the values at which stable Taylor vortices are anticipated. It may be observed, however, that  $Re_{cr}$  decreases drastically with the growth of the initial velocity  $v(0)$  as seen in Fig. 8. If  $v(0) > O(10)$ , the critical Reynolds number beyond which separation distance exhibits nonmonotonic behavior is much smaller, of the order of tens and hundreds. Note also that  $v(0)$  corresponds to the initial composite velocity of the bubble relative to the ambient fluid which is as it is in the experiments described in [5], where the bubbles were introduced into an already rotating fluid.

As in the case of the inviscid model, it follows from (41)–(43) that if  $v(0) = 0$ , then  $v(t) = 0 \forall t > 0$  and the evolution of  $l_1$  and  $u$  in the nonlinear system is governed by a second order autonomous system of ordinary differential equations. A phase

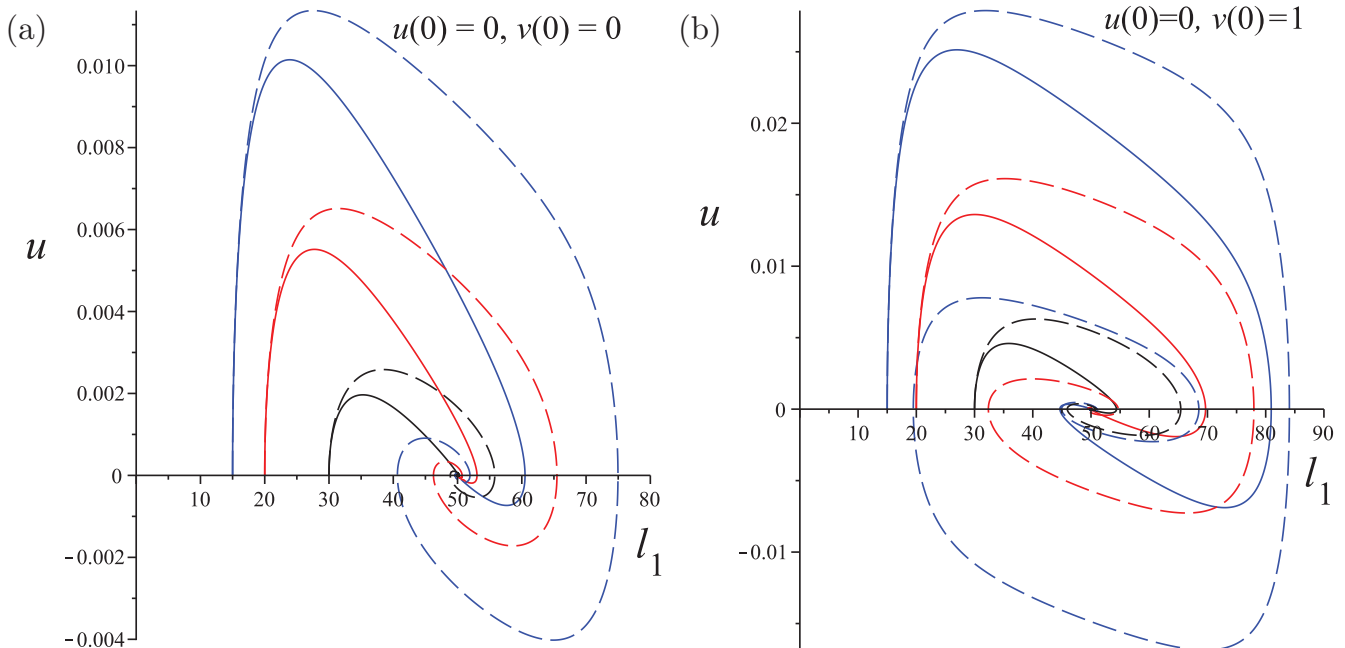


FIG. 9. (Color online) Phase space pattern at various initial conditions for the two bubble case. Solid and dashed lines correspond to the Reynolds numbers 60 000 and 120 000, respectively (two bubble case).

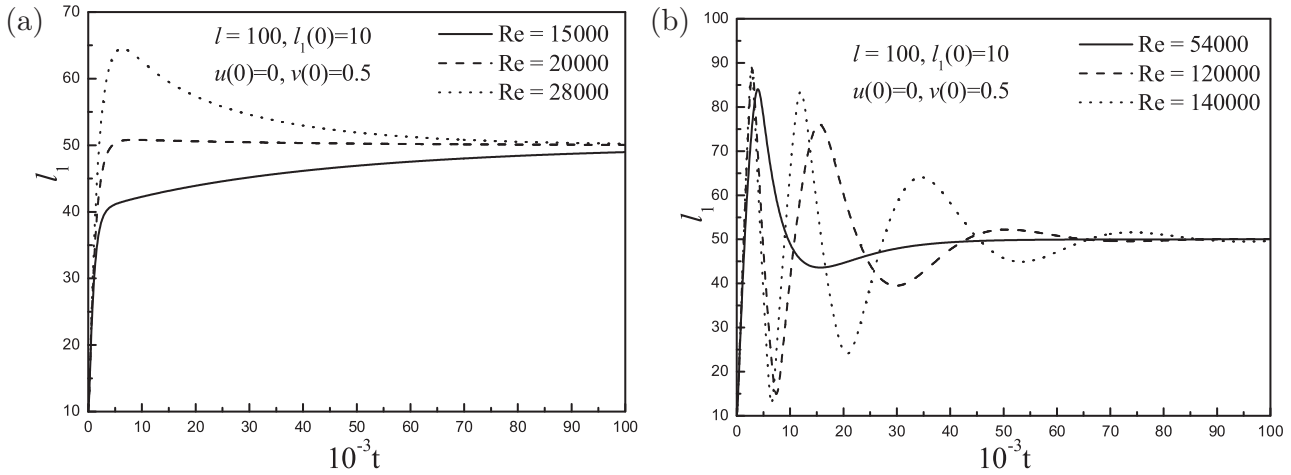


FIG. 10. Evolution of the separation distance between the bubbles (two bubble case): (a) Near  $Re_{cr} \simeq 19540$ , (b) high Reynolds number.

portrait of this system is presented in Fig. 9(a). Clearly, the fixed point is of the sink type and the motion is oscillatory with decreasing amplitude. With the passage of time the amplitude of the oscillations diminishes and bubble positions approach equilibrium. Figure 9(b) demonstrates the projection of the phase space to the plane  $(l_1, u)$  in the case of a nonzero  $v(0)$ . Solid and dashed lines correspond to  $Re = 60000$  and  $Re = 120000$ , respectively. The trajectories are qualitatively similar to the  $v = 0$  case. Note that the amplitude of oscillations varies with the initial conditions.

The evolution of the separation distance in the case of two bubbles is shown in Fig. 10 at various Reynolds numbers, where  $l = 100$ ,  $l_1(0) = 10$ ,  $u(0) = 0$ , and  $v(0) = 0.5$ . The solid curve in Fig. 10(a) represents the evolution at a Reynolds number below the critical one where the separation grows monotonically and slowly approaches equilibrium. The dashed curve in Fig. 10(a) corresponds to the case just above the critical Reynolds number, where the evolution shows an overshooting behavior as seen in several experimental runs reported in [5]. This nonmonotonic behavior becomes prominent as the Reynolds number increases, as demonstrated by the dotted curve in Fig. 10(a). From Fig. 10(a), one can see that, similar to the linear case, the relaxation time is minimal near critical situation.

With the further growth of  $Re$  beyond the critical value the separation distances of the bubbles start oscillating and the frequency of oscillations increases with increasing Reynolds number. As time elapses the oscillations diminish due to the viscous resistance, which causes a damping effect, and the bubbles assume equilibrium positions [Fig. 10(b)]. Note that the results in Fig. 10 are computed at high nonrealistic Reynolds numbers which are presented here to illustrate qualitative features of the model. At higher  $v(0)$  overshooting and oscillations appear at much lower  $Re$ , but the oscillations are much faster at the initial stage of the process and the relaxation is much slower than those depicted in Fig. 10.

It should be noted that there are several cases of initial relative and composite velocities for which bubbles may converge towards each other during the evolution of separation distance up to the point of possible collision which may cause

coalescence. Typical cases are those with a large enough initial relative velocity  $u(0)$ ; see, e.g., the case depicted in Fig. 11 by dashed and dotted curves.

An example of the evolution of the separation distances in the case of three bubbles having unequal initial separations is presented in Fig. 12 at various Reynolds numbers, where  $l = 100$ ,  $l_1(0) = 10$ ,  $l_2(0) = 15$  and where all the three bubbles have equal initial velocity of translation  $v_1 = v_2 = v_3 = 1.5$ . It can be seen from Figs. 12(a), 12(c), and 12(e) that at Reynolds number 4100 (solid curve), the initially minimal and maximal separation distances exhibit monotonic behavior, whereas the other separation distance exhibits overshooting, a behavior also predicted by the low-inertia analysis in [5]. However, as the Reynolds number increases all the separation distances exhibit oscillatory behavior and the frequency of oscillations increases with Reynolds number [dashed and dotted curves in Figs. 12(a), 12(c), 12(e) and all curves in Figs. 12(b), 12(d), 12(f)]. Note also that this oscillatory behavior can become quite complex [Fig. 12(d)]. The complex pattern seems to be prominent initially and beyond a certain time it becomes smooth and finally all the oscillations are damped and the bubbles achieve equilibrium positions.

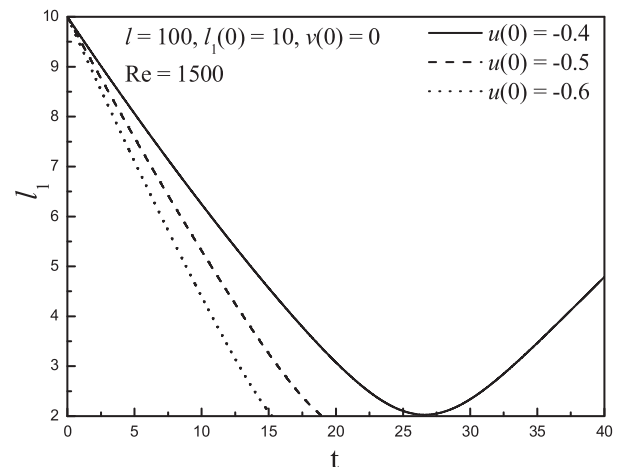


FIG. 11. Illustration of collision of bubbles (two bubble case).

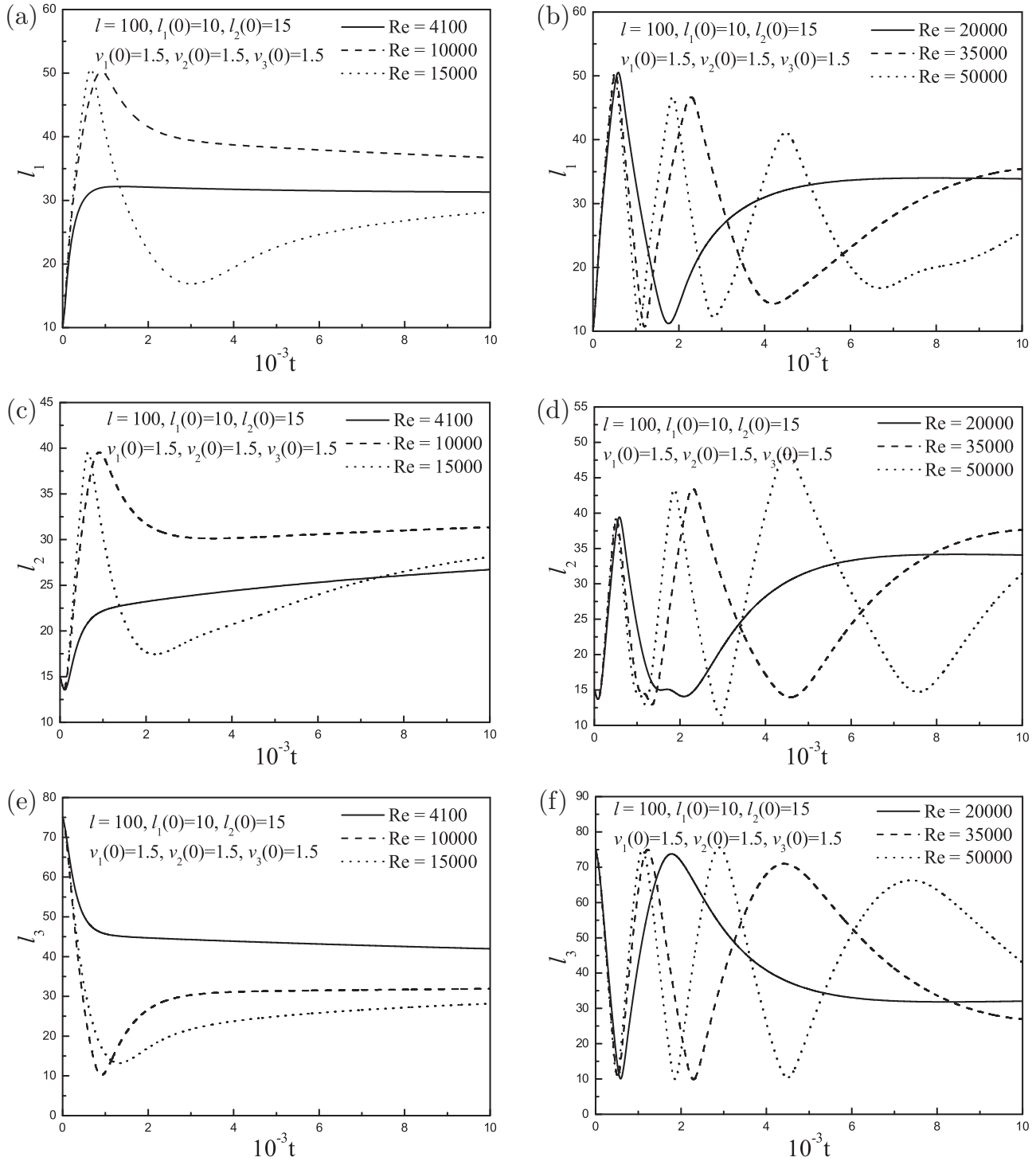


FIG. 12. Evolution of the separation distances between the bubbles at various Reynolds numbers (three bubble case).

The evolution of separations in the case of four bubbles is presented in Fig. 13 at various Reynolds numbers, where  $l = 100, l_1(0) = 5, l_2(0) = 15, l_3(0) = 35$  and where all the four bubbles have equal initial velocity of translation  $v_1 = v_2 = v_3 = v_4 = 1.2$ . As in the case of three bubbles at low Reynolds number, the initially minimal and maximal separation distances  $l_1$  and  $l_4$  in the four bubble case exhibit monotonic behavior, whereas the initially intermediate separation

distances  $l_2$  and  $l_3$  display nonmonotonic behavior [solid curve in Figs. 13(a), 13(c), 13(e), 13(g)]. Beyond some critical Reynolds number all the separation distances undergo oscillations with frequency that increases with the Reynolds number [dashed and dotted curves in Figs. 13(a), 13(c), 13(e), 13(g) and all curves in Figs. 13(b), 13(d), 13(f), 13(h)]. Also in this case the pattern of oscillations can exhibit complex behavior, as seen in Fig. 13(d). It may be noticed that the critical Reynolds

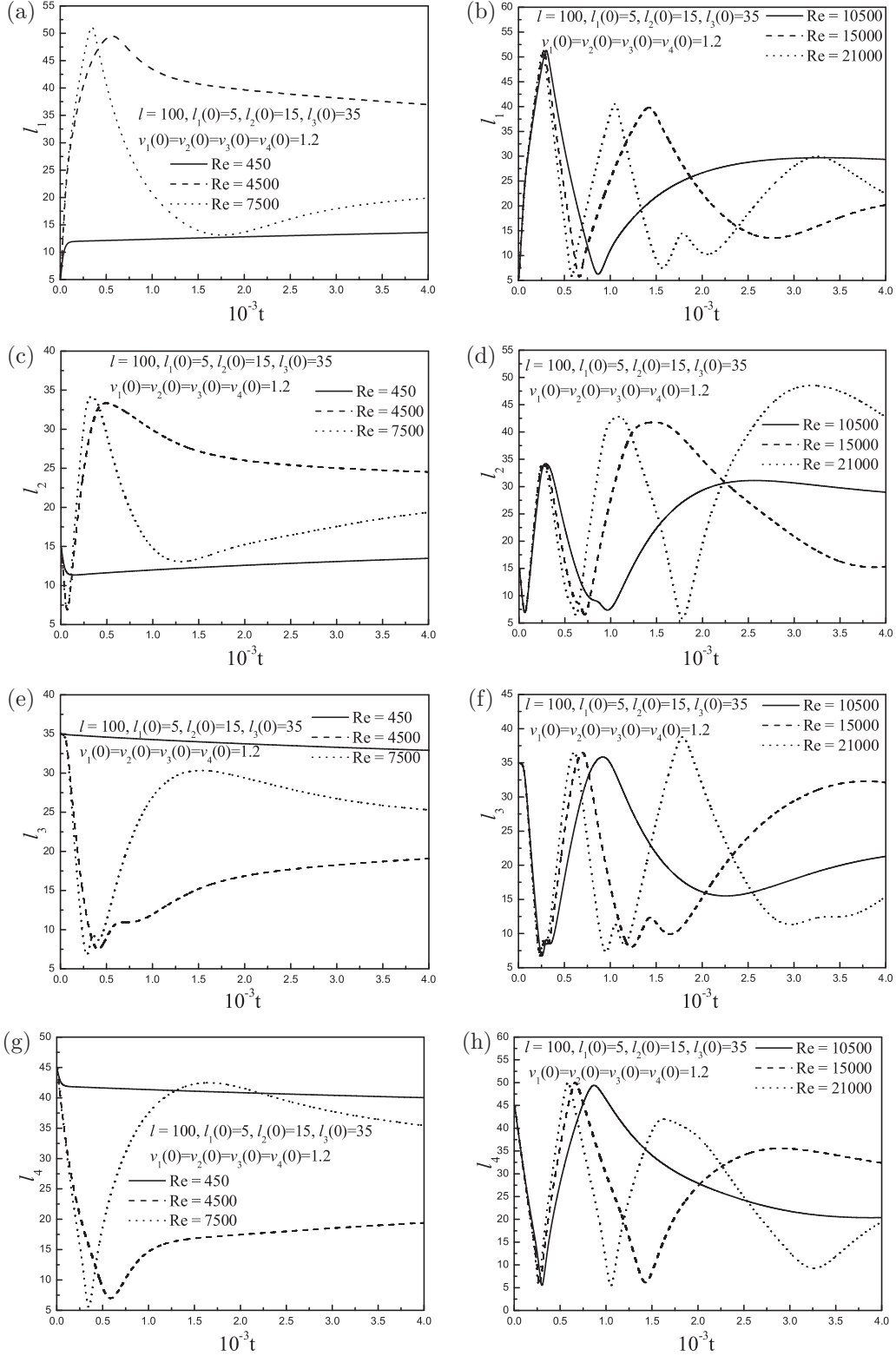


FIG. 13. Evolution of the separation distances between the bubbles at various Reynolds numbers (four bubble case).

number for the onset of oscillations decreases as the number of bubbles increases. Similarly, the relaxation time decreases as the number of bubbles increases as was also predicted in the case where viscous force was dominant over inertia [5] and in the linearized analysis presented above.

#### IV. CONCLUSIONS AND DISCUSSIONS

In this paper, we studied the effect of inviscid flow and of low viscosity on the evolution of separation between interacting bubbles in shear flow. We obtained the force acting

on bubbles, which was shown to be of a repulsive nature and was further employed to model the dynamics of the bubbles in a Couette-Taylor device. A simplified model of such dynamics is suggested where it is assumed that each bubble interacts solely with its nearest neighbors. We suggest also a low-viscosity model taking into account viscous dissipation effect at high Reynolds number. The application of the models results in systems of nonlinear ordinary differential equations describing the evolution of the separations between the bubbles.

The resulting systems of ordinary differential equations were studied by linearization in the vicinity of the equilibrium and by numerical integration of the nonlinear equations for various initial conditions in cases of two, three, and four bubbles. It was shown that, while in inviscid flow corresponding to infinite Reynolds number the bubbles undergo periodic motion, taking viscous resistance into account causes damping of these oscillations. As a result, oscillations diminish in time and bubbles achieve equilibrium configurations, with the relaxation time decreasing with an increase in the number of bubbles. The existence of a critical Reynolds number, below which no oscillations were observed, was found. Beyond the critical Reynolds number the separation distances start oscillating until the bubbles reach equilibrium positions. The pattern of oscillations in the supercritical regime, in the case of multiple bubbles, can become quite complicated, as is evident in Fig. 13.

The solution near stationary states obtained in the linear theory, describes the behavior of a system with a damping mechanism that is established at large time. Hence, it would apply to the cases discussed in Sec III B, and it provides a description of the behavior of the solution of the general nonlinear equations as time increases. It was shown that the linear theory predicts that the critical Reynolds number grows fast with the ratio of the length of streamline to the bubble radius. At  $l = O(100)$ , which is typical for the experiments described in [5],  $Re_{cr} = O(10^5)$ , at which values no stable Taylor vortices are anticipated. Thus, for the experimental conditions and in agreement with the experimental observations, our theory predicts monotonic approach to the equilibrium at developed stages of the process.

In simulations of the nonlinear equations, it was found that the critical Reynolds number drastically decreases with the growth of the initial velocity of the bubbles relative to that of the ambient fluid. It becomes of  $O(10)$  if quiescent bubbles are introduced into a moving fluid and the initial relative velocity equals that of the fluid at the center streamline in the Couette-Taylor device described in [5].

We conclude that the effects taken into account by our model can result in a nonmonotonic behavior of bubbles in a Couette-Taylor flow similar to those observed in several experimental runs reported in [5] that add further explanation to the low-viscosity model suggested there.

#### ACKNOWLEDGMENTS

The work was supported by Israel Science Foundation (Grant No. ISF/668.11). O.M.L. acknowledges the support

of the Israel Ministry of Immigrant Absorption. J.P. acknowledges partial support by a fellowship from Israel Council for Higher Education.

#### APPENDIX: BISPHERICAL COORDINATES

Consider the bispherical coordinate system connected with the two bubbles of radii unity as shown in Fig. 14 and linked with the cylindrical system  $(\rho, z, \phi)$  by the relation

$$\rho = \frac{c \sin \eta}{\cosh \xi - \cos \eta}, \quad z = \frac{c \sinh \xi}{\cosh \xi - \cos \eta}, \quad \phi = \phi, \quad (\text{A1})$$

where  $-\infty < \xi < \infty$ ,  $0 \leq \eta \leq \pi$ , and  $0 \leq \phi \leq 2\pi$  and  $c$  is related to the distance between the centers of bubbles,  $d$  by  $c = \frac{1}{2}\sqrt{d^2 - 4}$ . The interface of bubble 1 is described by the coordinate surface  $\xi = \alpha > 0$  and the interface of bubble 2 corresponds to  $\xi = -\alpha > 0$ , where  $\alpha$  is a constant given by  $\alpha = \sinh^{-1}(c)$ .

Following Lebedev [20], the solution of velocity potential, which is a harmonic function, is of the form

$$\Phi^{\text{shear}} = \frac{1}{c} \sum_{n=1}^{\infty} (\cosh \xi - \cos \eta)^{1/2} \left[ A_n \cosh \left( n + \frac{1}{2} \right) \xi + B_n \sinh \left( n + \frac{1}{2} \right) \xi \right] P_n^1(\cos \eta) \cos \phi, \quad (\text{A2})$$

where  $A_n$  and  $B_n$  are unknown constants to be determined from the boundary conditions and  $P_n^1$  are associated Legendre polynomials of degree  $n$  and order 1, respectively.

In order to determine the unknown constants  $A_n$  and  $B_n$ , the gradient of Eq. (A2) is computed in bispherical coordinate and substituted in the boundary condition (10). Then, the relations

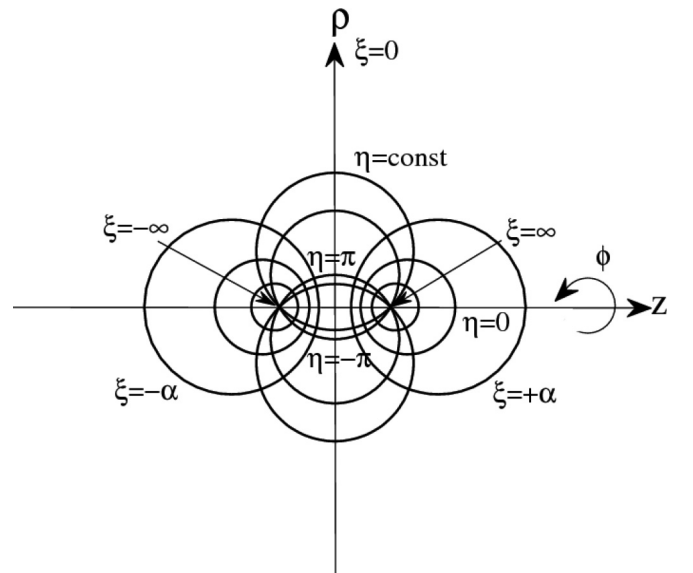


FIG. 14. Schematics of bispherical coordinate systems in  $(z, \rho)$  cylindrical coordinates plane. The coordinates  $\phi$  in cylindrical and bispherical systems coincide.

between associated Legendre polynomials are used to express both sides of the obtained equations in terms of  $P_n^1$ . These

equations are thus reduced to an infinite system of linear algebraic equations on the following coefficients:

(i) on  $\xi = \alpha$ ,

$$\begin{aligned}
 & -(n-1)A_{n-1} \sinh\left(n - \frac{1}{2}\right)\alpha + \left[ \sinh\alpha \cosh\left(n + \frac{1}{2}\right)\alpha + (2n+1) \cosh\alpha \sinh\left(n + \frac{1}{2}\right)\alpha \right] A_n \\
 & - (n+2)A_{n+1} \sinh\left(n + \frac{3}{2}\right)\alpha - (n-1)B_{n-1} \cosh\left(n - \frac{1}{2}\right)\alpha + \left[ \sinh\alpha \sinh\left(n + \frac{1}{2}\right)\alpha \right. \\
 & \left. + (2n+1) \cosh\alpha \cosh\left(n + \frac{1}{2}\right)\alpha \right] B_n - (n+2)B_{n+1} \cosh\left(n + \frac{3}{2}\right)\alpha \\
 & = \frac{4\sqrt{2}c^2}{\sinh\alpha} \left\{ - (n+2) \cosh\alpha \exp\left[-\left(n + \frac{3}{2}\right)\alpha\right] - (n-1) \cosh\alpha \exp\left[-\left(n - \frac{1}{2}\right)\alpha\right] \right. \\
 & \left. + (2n+1) \exp\left[-\left(n + \frac{1}{2}\right)\alpha\right] \right\}, \quad n = 1, \dots, \infty; \tag{A3}
 \end{aligned}$$

(ii) on  $\xi = -\alpha$ ,

$$\begin{aligned}
 & (n-1)A_{n-1} \sinh\left(n - \frac{1}{2}\right)\alpha - \left[ \sinh\alpha \cosh\left(n + \frac{1}{2}\right)\alpha + (2n+1) \cosh\alpha \sinh\left(n + \frac{1}{2}\right)\alpha \right] A_n \\
 & + (n+2)A_{n+1} \sinh\left(n + \frac{3}{2}\right)\alpha - (n-1)B_{n-1} \cosh\left(n - \frac{1}{2}\right)\alpha + \left[ \sinh\alpha \sinh\left(n + \frac{1}{2}\right)\alpha \right. \\
 & \left. + (2n+1) \cosh\alpha \cosh\left(n + \frac{1}{2}\right)\alpha \right] B_n - (n+2)B_{n+1} \cosh\left(n + \frac{3}{2}\right)\alpha \\
 & = \frac{4\sqrt{2}c^2}{\sinh\alpha} \left\{ - (n+2) \cosh\alpha \exp\left[-\left(n + \frac{3}{2}\right)\alpha\right] - (n-1) \cosh\alpha \exp\left[-\left(n - \frac{1}{2}\right)\alpha\right] \right. \\
 & \left. + (2n+1) \exp\left[-\left(n + \frac{1}{2}\right)\alpha\right] \right\}, \quad n = 1, \dots, \infty. \tag{A4}
 \end{aligned}$$

This system is truncated at some large  $N$  and is solved numerically using MATLAB. The accuracy is checked by repeating the procedure at  $2N$  and comparing the results. In a similar manner, the coefficients corresponding to the potential  $\Phi^{\text{trans}}$  and the auxiliary potential  $H$  can be obtained.

---

[1] J. Magnaudet and I. Eames, *Annu. Rev. Fluid Mech.* **32**, 659 (2000).  
 [2] E. Climent, M. Simonnet, and J. Magnaudet, *Phys. Fluids* **19**, 083301 (2007).  
 [3] R. Deng, C.-H. Wang, and K. A. Smith, *Phys. Rev. E* **73**, 036306 (2006).  
 [4] L. Byk, O. M. Lavrenteva, R. Spivak, and A. Nir, *Microgravity Sci. Technol.* **19**, 78 (2007).  
 [5] J. Prakash, O. M. Lavrenteva, L. Byk, and A. Nir, *Phys. Rev. E* **87**, 043002 (2013).  
 [6] D. Legendre and J. Magnaudet, *J. Fluid Mech.* **368**, 81 (1998).  
 [7] M. S. Howe, *Q. J. Mech. Appl. Math.* **48**, 401 (1995).  
 [8] H. Lamb, *Hydrodynamics* (Cambridge University Press, Cambridge, UK, 1945).  
 [9] G. K. Batchelor, *An Introduction to Fluid Dynamics* (Cambridge University Press, Cambridge, UK, 1967).  
 [10] L. Landweber and T. Miloh, *J. Fluid Mech.* **96**, 33 (1980).  
 [11] A. Galper and T. Miloh, *Phys. Fluids* **10**, 119 (1998).  
 [12] A. Galper and T. Miloh, *J. Fluid Mech.* **295**, 91 (1995).  
 [13] T. R. Auton, *J. Fluid Mech.* **183**, 199 (1987).  
 [14] T. R. Auton, J. C. R. Hunt, and M. Prud'Homme, *J. Fluid Mech.* **197**, 241 (1988).  
 [15] C. A. Catlin, *J. Fluid Mech.* **484**, 113 (2003).  
 [16] T. Miloh, *J. Fluid Mech.* **479**, 287 (2003).  
 [17] C. A. Catlin, *Int. J. Multiphase Flow* **30**, 455 (2004).  
 [18] A. Galper and T. Miloh, *Proc. R. Soc. London, Ser. A* **446**, 169 (1994).  
 [19] T. Miloh, *Phys. Fluids* **16**, 22 (2004).  
 [20] N. N. Lebedev, *Special Functions and Its Applications* (Dover, New York, 1972).  
 [21] R. Courant and D. Hilbert, *Methods of Mathematical Physics* (Wiley, New York, 1989), Vol. 2.  
 [22] J. Happel and H. Brenner, *Low Reynolds Number Hydrodynamics: With Special Applications to Particulate Media* (Kluwer Academic, Dordrecht, 1983).

- [23] V. G. Levich, *Zh. Eksp. Teor. Fiz.* **19**, 18 (1949).
- [24] V. G. Levich, *Physicochemical Hydrodynamics* (Prentice-Hall, Englewood Cliffs, NJ, 1962).
- [25] I. S. Kang and L. G. Leal, *Phys. Fluids* **31**, 233 (1988).
- [26] H. A. Stone, *Phys. Fluids A* **5**, 2567 (1993).
- [27] D. W. Moore, *J. Fluid Mech.* **16**, 161 (1963).
- [28] J. L. S. Chen, *Trans. ASME J. Appl. Mech.* **41**, 873 (1974).
- [29] S. G. Slavchev and G. Simeonov, *Z. Angew. Math. Mech.* **59**, 43 (1979).
- [30] J. Magnaudet and D. Legendre, *Phys. Fluids* **10**, 550 (1998).